Available online at www.sciencedirect.com

ScienceDirect

Green Energy & Environment 2 (2017) 278–284

www.keaipublishing.com/gee

Research paper

Ultra-light and flexible pencil-trace anode for high performance potassium-ion and lithium-ion batteries

Zhixin Tai [a,1], Yajie Liu [a,1], Qing Zhang [a,1], Tengfei Zhou [a], Zaiping Guo [a,b,*], Hua Kun Liu [a], Shi Xue Dou [a]

[a] *Institute for Superconducting and Electronic Materials, Australian Institute for Innovative Materials, University of Wollongong, Innovation Campus, North Wollongong, NSW 2500, Australia*

[b] *School of Mechanical, Materials and Mechatronics Engineering, University of Wollongong, North Wollongong, NSW 2500, Australia*

Received 3 March 2017; revised 20 April 2017; accepted 21 April 2017
Available online 27 April 2017

Abstract

Engineering design of battery configurations and new battery system development are alternative approaches to achieve high performance batteries. A novel flexible and ultra-light graphite anode is fabricated by simple friction drawing on filter paper with a commercial 8B pencil. Compared with the traditional anode using copper foil as current collector, this innovative current-collector-free design presents capacity improvement of over 200% by reducing the inert weight of the electrode. The as-prepared pencil-trace electrode exhibits excellent rate performance in potassium-ion batteries (KIBs), significantly better than in lithium-ion batteries (LIBs), with capacity retention of 66% for the KIB *vs.* 28% for the LIB from 0.1 to 0.5 A g^{-1}. It also shows a high reversible capacity of ~230 mAh g^{-1} at 0.2 A g^{-1}, 75% capacity retention over 350 cycles at 0.4 A $g^{-1}$and the highest rate performance (based on the total electrode weight) among graphite electrodes for K^+ storage reported so far.

Keywords: Current-collector-free; Flexible pencil-trace electrode; Potassium-ion battery; Lithium-ion battery; Layer-by-layer interconnected architecture

1. Introduction

The demand for lithium-ion batteries (LIBs), as the most important power supply for electronic devices, is rapidly increasing [1,2]. Limited lithium resources, which are unevenly distributed around the world, have resulted in rising costs for their future large-scale commercialization [3]. Therefore, tremendous growing interest has been focused on the alternative earth-abundant metal ion batteries, including sodium-ion batteries (NIBs), potassium-ion batteries (KIBs), etc. [4–7] As reported, graphite anode exhibits a higher theoretical capacity (~270 mAh g^{-1}) in KIBs than in NIBs (~35 mAh g^{-1}), indicating that the KIBs may be a better candidate than NIBs for commercial graphite anode [6]. So, in this work, we present a comparative study of both KIBs and LIBs based on graphite anode material.

Slurry-casting is commonly used for electrode fabrication, in which active materials, binders, and carbon-conductive additives are cast onto metal foil. The main roles of the current collector are to provide mechanical support and collect current from the electrode. Current collectors could be avoided if the electrode is intrinsically self-supported and has good electrical conductivity. It is obvious that a current-collector-free electrode can significantly reduce the electrode weight and space, and could be an effective strategy for promoting the energy density of batteries [8,9].

* Corresponding author. Institute for Superconducting and Electronic Materials, Australian Institute for Innovative Materials, University of Wollongong, Innovation Campus, North Wollongong, NSW 2500. Australia.
E-mail address: zguo@uow.edu.au (Z. Guo).

[1] These authors contributed equally to this work.

http://dx.doi.org/10.1016/j.gee.2017.04.002

In addition, flexibility of electrodes and mechanical compatibility of different components in the electrodes are crucial for large-scale electrode processing and battery assembly. There are two approaches to developing current-collector-free flexible electrodes: the use of an active material that is intrinsically flexible, or the use of composite electrodes with flexible supports. Intrinsically flexible electrodes that are so far known typically use self-standing carbon-based materials such as one-dimensional (1D) carbon nanotubes (CNTs), two-dimensional (2D) graphene, or some electroactive polymers [10–12]. One such example uses graphene paper as a functional material, which not only acts as a conducting agent, but also as a current collector [13]. The as-prepared film electrode is often slightly brittle with limited flexibility, especially in large pieces, and the fabrication process is always complicated and time-consuming, which makes its large-scale fabrication and application infeasible [14]. Flexible composite electrodes combine conventional high-energy-density active materials with flexible supports, including CNTs or graphene paper, polymers, or cotton [14–17]. For achieving simple electrode fabrication with each part intact and in contact, compatibility between the components and mechanical flexibility is still a challenge for the flexible composite electrodes [16].

Pencil drawing on a substrate is a solvent-free technique to obtain continuous flexible films, which display good conductivity and adhesion strength [16]. Flexible films made via pencil drawing have been successfully adopted in many devices, including Li-ion and Li-air batteries, supercapacitors, strain/gas sensors, field electron emitters, and field effect transistors with outstanding performance [18–21]. Inspired by its low-cost and simple fabrication, herein, we have developed a current-collector-free pencil-trace/filter paper electrode by directly drawing on the separator for the first time. Compared with the reported pencil-traces on copper foil electrode [9], we not only achieved high-mass-loading of the active material on the rough surface of the filter paper with strong adhesion, but also achieved high-energy-density batteries by introducing a novel current-collector-free design. The as-prepared pencil-trace electrode exhibited excellent rate performance in KIBs, which was much superior to that in LIBs, with capacity retention of 66% for the KIB *vs.* 28% for the LIB from 0.1 to 0.5 A g^{-1}. It also exhibited 75% capacity retention over 350 cycles at a current density of 0.4 A g^{-1} and higher rate performance than any other graphite electrode for K^+ storage reported so far.

2. Experimental section

2.1. Preparation of pencil-trace electrode

The separator used in this study was commercially available filter paper (ADVANTEC). To prepare the pencil-trace electrode, an 8B-grade pencil (STAEDTLER, Germany) purchased from Office Works was used as the active material resource. After a simple modification of the coating machine (Hohsen, MC20), as shown in Fig. 1c–e, the pencil was fixed on the holder of the coating machine so as to control the thickness of the pencil-trace by drawing repeated lines, and the coating speed of 2.5 mm s^{-1} was used to control the uniformity of the pencil-trace. After drawing a line, the pencil was adjusted carefully again with the same parameters to draw another line next to the previous one to cover the substrate surface. Finally, the overlapping pencil-drawn lines produced a graphite film on the filter paper. Then, the as-prepared pencil-trace/filter paper was cut into small disks with 19 mm in diameter for fabricating the cells. The mass loading of the pencil-trace is around 0.5–1.0 mg cm^{-1}.

2.2. Materials characterization

The crystal structure of the powder products was examined by X-ray diffraction (XRD) (MMA GBC, Australia) with Cu Kα radiation. Fourier-transform infrared spectroscopy (FT-IR) and X-ray photoelectron spectroscopy (XPS) analysis were carried out to characterize the chemical composition of the samples. X-ray photoelectron spectra (XPS) were collected on a Thermo Fisher K-alpha XPS spectrometer. The microstructure of the fabricated pencil-trace was investigated with a Raman system (Thermo Nicolet Almega XR Raman Microscope, with the excitation wavelength at 532.81 nm). Scanning electron microscope (SEM) images were obtained with a JEOL JSM-7500 microscope. High resolution transmission electron microscope (HRTEM) images were obtained using an aberration-corrected JEOL ARM-200F (JEOL, Corrector: CEOS) operating at 200 kV. The microscope is equipped with a JED-2300 (JEOL) energy-dispersive X-ray spectrometer (EDS).

2.3. Electrochemical measurements

The electrode was dried at 120 °C under vacuum for 12 h before assembling. Coin cells (CR2032) were assembled with potassium foil as the counter/reference electrode, the pencil-trace/filter paper composite film as separator and active material electrode, and 0.8 M KPF_6 in ethylene carbonate/diethyl carbonate (EC/DEC, 1:1 v/v) as the electrolyte for the potassium-ion battery and 1.0 M $LiPF_6$ in ethylene carbonate/diethyl carbonate (EC/DEC, 1:1 v/v) for the lithium-ion battery in an argon-filled glove box. Charge/discharge measurements were carried out on a Neware battery test system, model BTS-XWJ-6.44S-00052 (Neware, Shenzhen, China), at different current densities between 0 and 2 V *vs.* K/K^+ and Li/Li^+ at room temperature.

3. Results and discussion

Here, an ultra-light electrode designed with a reduced amount of inactive component was proposed (Fig. 1a). In order to preserve the high-energy-density, while offering good flexibility of the electrode, a solvent-free fabrication technique, namely, pencil drawing, was employed to prepare the metal-current-collector-free electrode fabricated by drawing lines on commercially available filter paper (Fig. 1c–e). The

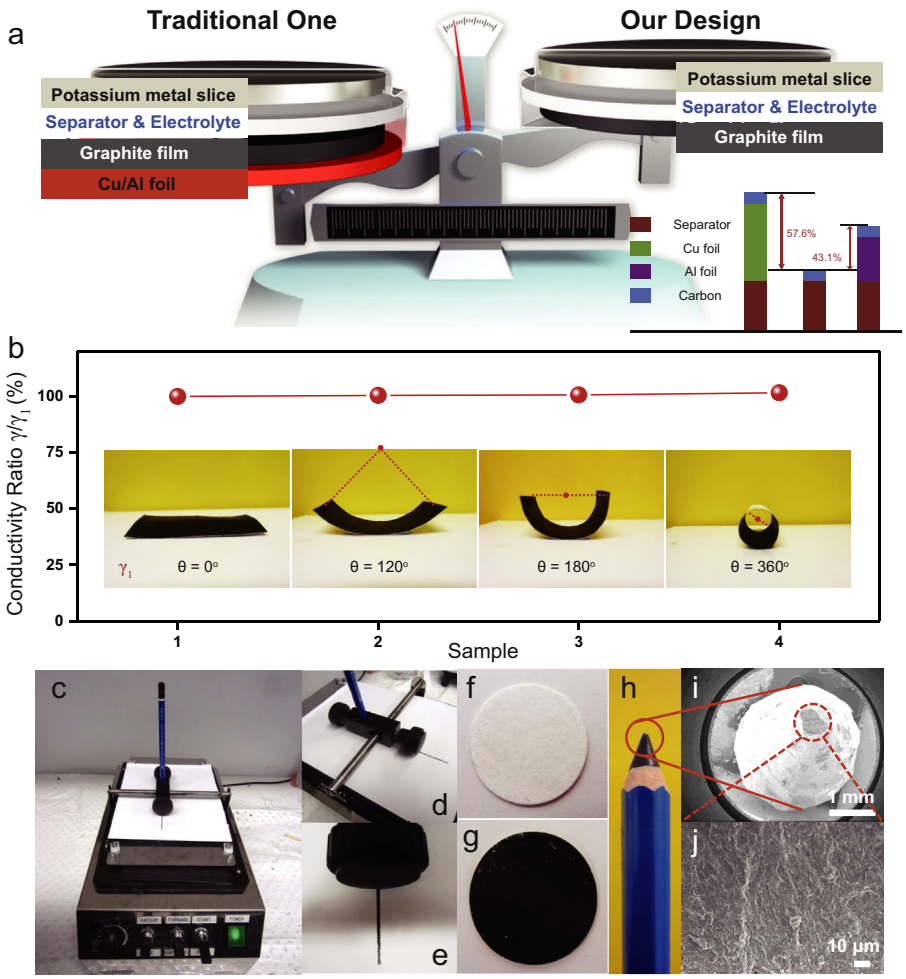

Fig. 1. (a) Schematic illustration of the novel ultra-light electrode design compared with a traditional electrode; (b) Stability of an integrated flexible pencil-trace/filter paper electrode in terms of conductivity variation with different bending angles; (c) Photograph of the converted pencil drawing machine with detailed photographs of the fixed pencil apparatus (d) and pencil-trace line (e); Filter paper separator before (f) and after pencil-trace coating (g); (h) Commercial 8B pencil; (i–j) SEM images at different magnifications of the point of the pencil lead.

resultant pencil-trace/filter paper composite film has a uniform black color and the pencil lead shows a wrinkled and rough surface, as shown in Fig. 1f–j. The intactness of the flexible electrode under different degrees of bending is a guarantee of its practical use, which can be verified by testing the electrical properties under mechanical deformations. The dynamic electrical properties of this pencil-trace electrode were investigated by measuring the electrical conductivity changes after bending the electrode to different angles. As shown in Fig. 1b, the specific conductivity remains almost unchanged at different bending angles, indicating the excellent flexibility, and strong adhesion between the pencil-trace and the separator. Its light-weight, mechanically robust nature, and high flexibility allow it to be used as a high-energy flexible anode.

The morphology and composition of the pencil-trace were characterized by scanning electron microscopy (SEM) and scanning transmission electron microscopy (STEM). Fig. S1 in the Supporting Information shows the porous structure of the filter paper with some fibers distributed irregularly in the paper. This rough surface of the paper enables the exfoliation, transfer, and adhesion of graphite from the pencil. Compared with the rough surface of the filter paper, the pencil-trace electrode shows a relatively flat and dense morphology, indicating that the pencil-trace formed a uniform coating. As shown in a high-resolution SEM image (Fig. 2a), the friction direction can be determined by the trace formed from the sliding pencil. Actually, the advance of the pencil-trace involves the formation of a transferred film through friction (see Fig. S2) [22]. Specifically, the reciprocating motion of the pencil lead under some load could generate considerable wear debris (graphite and solid clay binder) by shearing. Following the sliding, the solid binder would absorb the graphite debris and form a new graphite film on the filter paper. Fig. 2b shows a cross-sectional image of the generated graphite film on the separator, in which adhesion between the pencil-trace film (thickness: 30 μm) and the separator (~150 μm) is significantly improved by friction coating via pencil drawing. The thickness of the pencil-trace on the filter paper is controllable and adjustable, depending on the layers of pencil-drawn lines, which could straightforwardly achieve a high-mass-loading

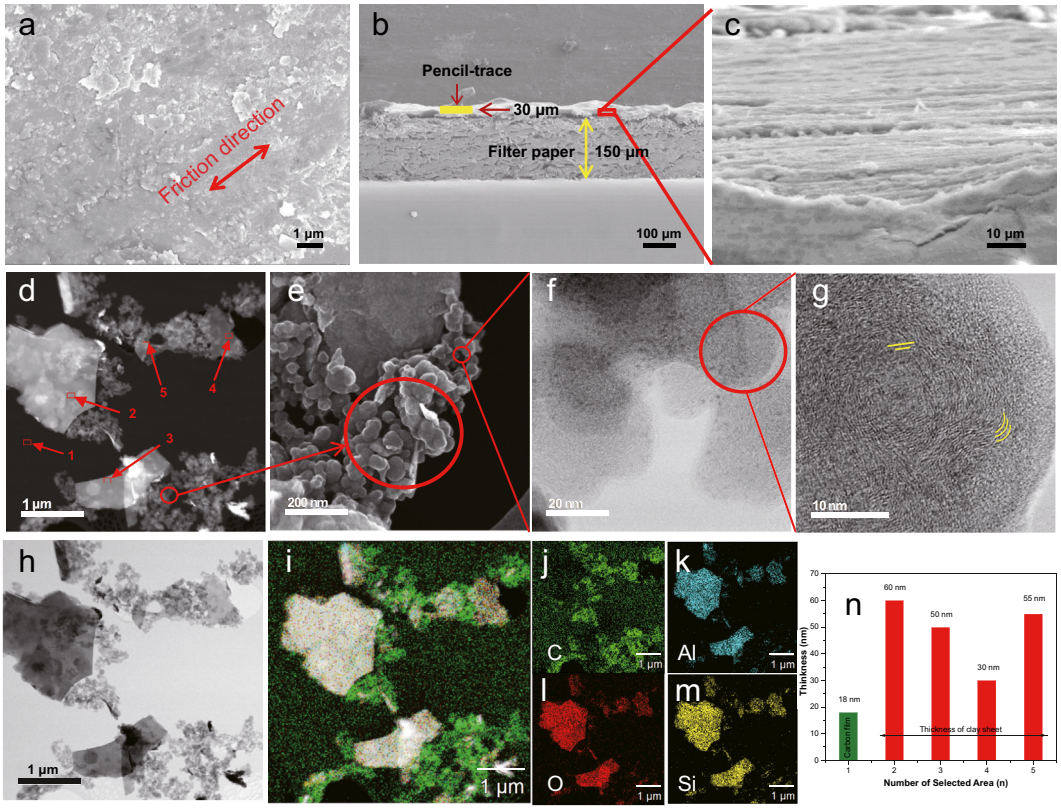

Fig. 2. Morphology and microstructure of the as-prepared pencil-trace: (a) The top-view SEM image, (b) cross-sectional image, and (c) high-resolution cross-section image of pencil-trace/filter paper; (d–g) STEM images of the graphite particles in the pencil-trace at different magnifications. (h) STEM image of pencil-trace composite under Z-contrast transmission mode; (i–m) corresponding EDX mapping images of the C, Al, O, and Si, respectively. (n) Thickness histogram of the selected clay nanosheets as indicated in the Figure 2d.

flexible electrode (Fig. S3). The STEM images in Fig. 2d–e reveal that the hierarchical structured film consists of nanosheets and nanoparticles (Fig. 1g). Due to the binder effect of clay, the clay and graphite particles are likely to be incorporated together to form a layer-by-layer structured film, as shown in Fig. 2c. Energy dispersive spectroscopy (EDS) mapping shows the uniform distribution of aluminum, oxygen, and silicon on the nanosheets, while carbon is the main element from the nanoparticles, indicating the flake morphology of the clay and that the nanoparticles are graphite in the pencil-trace. The thicknesses of clay samples (average thickness around 50 nm) are shown in Fig. 2n, based on the different selected sheets in Fig. 2d. Here, the graphite nanoparticles are assembled around the clay sheets and form an interconnected conducting network, facilitating fast charge transfer. The interconnected graphite with high surface area could provide large amounts of active sites for insertion/de-insertion of K^+ and Li^+ ions.

X-ray diffraction (XRD) was conducted to investigate the electrode's structural characteristics. As shown in Fig. 3a, the XRD pattern of the pencil-trace film shows a characteristic peak at around 26.5°, corresponding to commercial graphite with *d*-spacing of ~3.34 Å [23]. Moreover, SiO_2, as the major phase of clay, has peaks that agree well with the standard reference (00-002-047) [9]. Fig. 3b presents the Raman spectra of the pencil-trace and commercial graphite. In the case of the pencil-trace, the characteristic peaks of the G and D bands appear at around 1580 and 1350 cm^{-1}, respectively [24]. The intensity ratio I_D/I_G ($\approx$1.1) for the pencil-trace is much higher than for graphite, indicating that the pencil-trace has a higher degree of disorder than graphite [25]. According to the XPS spectrum presented in Fig. 3c, the main elements in the pencil-trace are C, O, Al, and Si, respectively, which is in good agreement with the EDS results for the pencil-trace [26]. In the C 1s XPS spectrum, the graphite C (284.6 eV) is dominant in the pencil-trace, and the rest of the carbon element in the pencil-trace is mainly in the forms of C–O (286.0 eV) [27] and C=O (287.6 eV) [28] groups (Fig. 3d).

The electrochemical performance of the pencil-trace anode was investigated in a half-cell configuration, using potassium metal or lithium metal as the counter electrode. Cyclic voltammetry (CV) measurements were carried out at a scan rate of 0.5 mV s^{-1}. As shown in Fig. S4, a broad peak near 0.7 V only exists in the first cathodic process, which is attributed to the decomposition of the electrolyte and the formation of the solid electrolyte interphase (SEI) film. The sharp cathodic peak between 0.3 and 0.01 V is related to the intercalation of K^+ into graphite, while the broad peak between 0.3 and 0.8 V corresponds to the deintercalation of K^+ from the pencil-trace. Furthermore, the other cathodic/anodic peaks are reversible

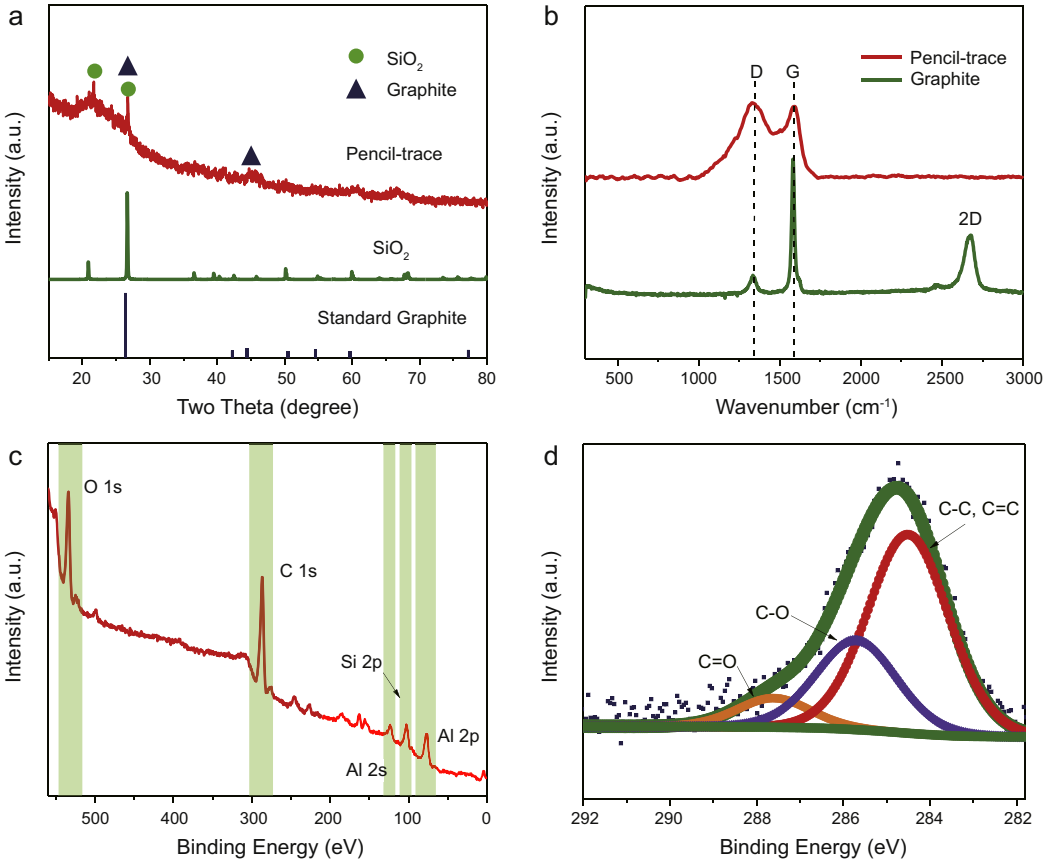

Fig. 3. Characteristics of the pencil-trace: (a) XRD pattern and (b) Raman spectrum of the pencil-trace compared with pure graphite; (c) XPS survey spectrum of the pencil-trace; (d) C 1s XPS spectrum for the pencil-trace.

and overlapping, indicating the high reversibility of the intercalation/deintercalation of K^+ into/from the pencil-trace. The rate capability of the pencil-trace was investigated against potassium and lithium at various current densities, as shown in Fig. 4a. The capacity was calculated based on the mass of graphite active material (accounting for 60 wt% in the pencil-trace, as shown in Fig. S5). Although its capacity at a low current density is lower in KIBs than in LIBs, as the current density rises above 0.5 A g^{-1}, its capacity in KIBs starts to exceed that in LIBs and shows outstanding rate performance, indicating the higher kinetics of the K^+ intercalation process compared to the Li^+. In the case of the pencil-trace electrode for KIBs in Fig. 4b, capacity retention of 66% was obtained from 0.1 to 0.5 A g^{-1}, while in LIBs, capacity retention was only 28% within the same range. The cycling performance of the pencil-trace in KIBs and LIBs at a current density of 0.4 A g^{-1} is presented in Fig. 4d. The cycling stability of the pencil-trace electrode in both KIBs and LIBs are excellent (93% capacity retention for the KIB *vs.* 81% for the LIB from the 50^{th} to the 350^{th} cycle). Not only does the pencil-trace electrode present superiority in rate performance and cycling stability in KIBs compared with LIBs, the pencil-trace electrode for KIBs also shows greater safety than for NIBs in terms of the metal dendrite issues. Compared with the sodiation and desodiation peaks (0.1 V and 0.05 V) reported for a hard carbon/Na cell [29], the potassiation and depotassiation peaks are at 0.12 and 0.33 V versus K^+/K for the pencil-trace electrode, as shown in the *dQ*/*dV* profile (Fig. S6). When metal ion insertion occurs at potentials too close to the plating of the corresponding metal, dendrite formation can be a serious concern, particularly at high current rates, suggesting that KIBs are suprior to NIBs in terms of the safety concerns. In order to present the advantages of our current-collector-free electrode, we compared the capacity of the pencil-trace based on the mass with and without copper foil or aluminum foil (Fig. 4c). The capacity of the pencil-trace/separator shows almost 235% and 176% improvement over that of the pencil-trace + separator + copper foil and the pencil-trace + separator + aluminum foil electrodes, respectively, for both KIBs and LIBs. The electrochemical performance of the pencil-trace was also compared with that of graphite in KIBs (Fig. 4e–f). After 350 cycles, the pencil-trace electrode still shows sustained capacity retention of ~75% at current density of 0.4 A g^{-1}, while it drops to nearly 25 mAh g^{-1} in the pure graphite anode. Fig. S7 shows the galvanostatic charge/discharge profiles of the pencil-trace electrode at a current density of 0.4 A g^{-1}. The profiles of the 50th, 100th, 150th, 250th, and 350th cycles nearly overlap with each other, showing that the capacity decay is nearly zero between the 50th and 350th cycles. Even after 350 cycles, there is barely any change in the electrode morphology and no obvious cracking at low magnification, indicating the good stability of

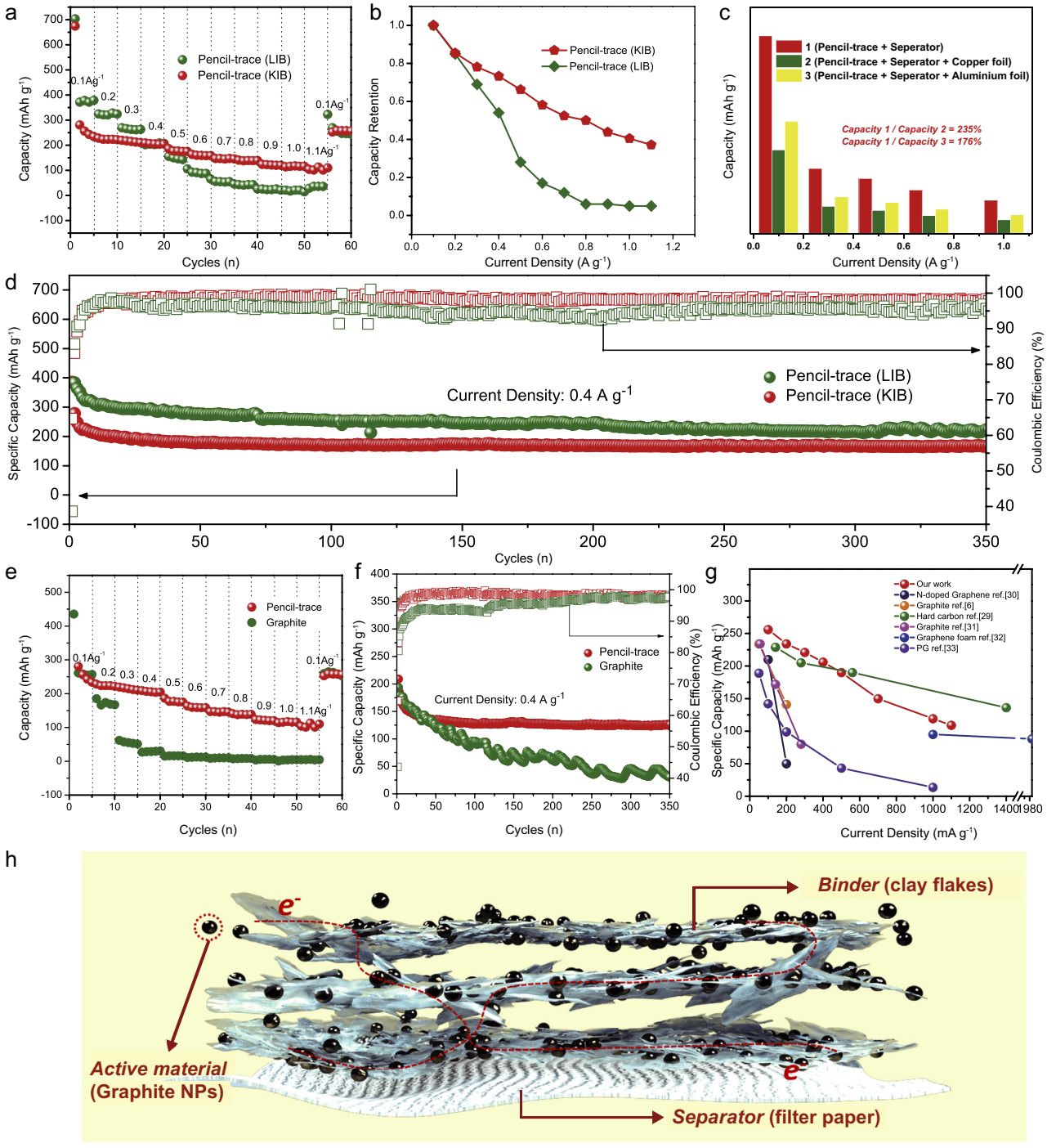

Fig. 4. Comparison of electrochemical performance (EC) of pencil-trace electrode in KIB and LIB cells: (a) rate performance; (b) capacity retention at various current densities; (c) comparison of different electrode configurations (pencil-trace + separator, pencil-trace + copper foil + separator, and pencil-trace + separator + aluminum foil). (d) Cycling performance at current density of 0.4 A g^{-1}. EC comparison of pencil-trace anode and commercial graphite anode in KIBs: (e) Rate performance at current density from 0.1 A g^{-1} (~0.36 C) to 1.1 A g^{-1} (~3.9 C); (f) Long-term cycling performance at current density of 0.4 A g^{-1}. (g) Capacity plot of various carbon-based electrodes for KIBs [6,29–33]. (Note that all the reported capacities of carbon-based electrodes are calculated based on the active material mass. Our work would be the highest one if the capacity calculation were based on the total electrode mass including the current collector.) (h) Schematic illustration of the layer-by-layer architecture of the pencil-trace electrode.

the pencil-trace electrode (Fig. S8). The electrochemical performances of all the state-of-the-art carbon-based electrodes for the potassium-ion battery were compared with our work, as shown in Fig. 4g. Among all the carbon-based anodes [6,29–33], the pencil-trace electrode could deliver the competitive rate performance among them, whether the specific capacity was calculated based on the active material or the total weight of the electrode, including the current

collector. The outstanding electrochemical performance of the pencil-trace electrode in KIBs compared with other graphite anodes can be attributed to the unique three-dimensional (3D) layer-by-layer interconnected architecture, which combines 2D clay sheets and graphite nanoparticles (Fig. 4h). This unique structure could facilitate charge transfer [34,35], and the high surface area of the pencil-trace electrode could provide more active sites for reaction with K^+. Compared with the traditional electrode fabrication by slurry-casting, the pencil-trace on filter paper is assembled layer-by-layer by pencil drawing, which guarantees the integrity of the electrode and the uniformity of each electrode component.

4. Conclusion

In summary, we have demonstrated an ultra-light and flexible pencil-trace electrode for the lithium-ion battery and potassium-ion battery via employing a pencil drawing technique. This novel electrode design not only achieves an electrode with high mechanical flexibility and an adjustable loading mass, but also enhances the gravimetric energy density by decreasing the weight of the inactive part of the electrode. A comparison of the electrochemical performance of LIBs and KIBs is inspiring. The superiority of the pencil-trace electrode in KIBs, in such aspects as high rate performance, reasonable capacity (improved by the current-collector-free design), and excellent cycling stability, makes the potassium-ion battery a potential alternative to the lithium-ion battery. Moreover, the pencil-trace electrode also presents better electrochemical performance than other reported carbon-based anodes in KIBs. This could be due to the layer-by-layer interconnected architecture combining 2D clay sheets and graphite nanoparticles, which facilitates K^+ diffusion and charge transfer to some extent.

Conflict of interest

There is no conflict of interest.

Acknowledgements

Support from the Australian Research Council through a Discovery project (DP170102406) and Future Fellowship project (FT150100109), and Auto CRC 2020 (Project 1-117) are gratefully acknowledged. This research used equipment funded by an Australian Research Council grant (LE0237478), with the facilities located at the UOW Electron Microscopy Centre. Many thanks are owed to Dr. Tania Silver for critical reading of the manuscript.

Appendix A. Supplementary data

Supplementary data related to this article can be found at http://dx.doi.org/10.1016/j.gee.2017.04.002.

References

[1] Q. Zhao, Y. Lu, Z. Zhu, Z. Tao, J. Chen, Nano Lett. 15 (2015) 5982–5987.
[2] Y. Xu, Y. Zhu, Y. Liu, C. Wang, Adv. Energy Mater. 3 (2013) 128–133.
[3] B. Dunn, H. Kamath, J.M. Tarascon, Science 334 (2011) 928–935.
[4] J. Qian, X. Wu, Y. Cao, X. Ai, H. Yang, Angew. Chem. Int. Ed. Engl. 52 (2013) 4633–4636.
[5] C. Chen, Y. Wen, X. Hu, X. Ji, M. Yan, L. Mai, P. Hu, B. Shan, Y. Huang, Nat. Commun. 6 (2015) 6929.
[6] Z. Jian, W. Luo, X. Ji, J. Am. Chem. Soc. 137 (2015) 11566–11569.
[7] S. Komaba, T. Hasegawa, M. Dahbi, K. Kubota, Electrochem. Commun. 60 (2015) 172–175.
[8] H. Gwon, H.S. Kim, K.U. Lee, D.H. Seo, Y.C. Park, Y.S. Lee, B.T. Ahn, K. Kang, Energy Environ. Sci. 4 (2011) 1277–1283.
[9] H.Y. Park, M.S. Kim, T.S. Bae, J. Yuan, J.S. Yu, Langmuir 32 (2016) 4415–4423.
[10] X. Xiao, T. Li, Z. Peng, H. Jin, Q. Zhong, Q. Hu, B. Yao, Q. Luo, C. Zhang, L. Gong, J. Chen, Y. Gogotsi, J. Zhou, Nano Energy 6 (2014) 1–9.
[11] P. Li, Y. Yang, E. Shi, Q. Shen, Y. Shang, S. Wu, J. Wei, K. Wang, H. Zhu, Q. Yuan, A. Cao, D. Wu, ACS Appl. Mater. Interfaces 6 (2014) 5228–5234.
[12] K. Wang, H. Wu, Y. Meng, Z. Wei, Small 10 (2014) 14–31.
[13] K. Rana, J. Singh, J.T. Lee, J.H. Park, J.H. Ahn, ACS Appl. Mater. Interfaces 6 (2014) 11158–11166.
[14] B. Dan, G.C. Irvin, M. Pasquali, ACS Nano 3 (2009) 835–843.
[15] P. Chen, H. Chen, J. Qiu, C. Zhou, Nano Res. 3 (2010) 594–603.
[16] G. Zheng, L. Hu, H. Wu, X. Xie, Y. Cui, Energy Environ. Sci. 4 (2011) 3368–3373.
[17] L. Hu, H. Wu, Y. Cui, Appl. Phys. Lett. 96 (2010) 183502.
[18] Y. Wang, H. Zhou, Energy Environ. Sci. 4 (2011) 1704–1707.
[19] X. Liao, Q. Liao, X. Yan, Q. Liang, H. Si, M. Li, H. Wu, S. Cao, Y. Zhang, Adv. Funct. Mater. 25 (2015) 2395–2401.
[20] N. Kurra, D. Dutta, G.U. Kulkarni, Phys. Chem. Chem. Phys. 15 (2013) 8367–8372.
[21] J. Chen, B. Yang, X. Liu, J. Yang, X. Yan, Appl. Phys. Lett. 108 (2016) 193112.
[22] S.F. Moustafa, S.A. El-Badry, A.M. Sanad, B. Kieback, Wear 253 (2002) 699–710.
[23] F. Razmjooei, K.P. Singh, M.Y. Song, J.S. Yu, Carbon 78 (2014) 257–267.
[24] W. Zhao, P.H. Tan, J. Liu, A.C. Ferrari, J. Am. Chem. Soc. 133 (2011) 5941–5946.
[25] A.C. Ferrari, J. Robertson, Phys. Rev. B 61 (2000) 14095–14107.
[26] R.N. Bhowmik, Compos. Part B Eng. 43 (2012) 503–509.
[27] Z. Wu, P.A. Webley, D. Zhao, J. Mater. Chem. 22 (2012) 11379–11389.
[28] Y. Tao, X. Xie, W. Lv, D.M. Tang, D. Kong, Z. Huang, H. Nishihara, T. Ishii, B. Li, D. Golberg, F. Kang, T. Kyotani, Q.H. Yang, Sci. Rep. 3 (2013) 2975.
[29] Z. Jian, Z. Xing, C. Bommier, Z. Li, X. Ji, Adv. Energy Mater. 6 (2016) 1501874.
[30] K. Share, A.P. Cohn, R. Carter, B. Rogers, C.L. Pint, ACS Nano 10 (2016) 9738–9744.
[31] W. Luo, J. Wan, B. Ozdemir, W.Z. Bao, Y. Chen, J. Dai, H. Lin, Y. Xu, F. Gu, V. Barone, L. Hu, Nano Lett. 15 (2015) 7671–7677.
[32] A.P. Cohn, N. Muralidharan, R. Carter, K. Share, L. Oakes, C.L. Pint, J. Mater. Chem. A 4 (2016) 14954–14959.
[33] Z. Xing, Y. Qi, Z. Jian, X. Ji, ACS Appl. Mater. Interfaces 9 (2017) 4343–4351.
[34] J. Zhu, Z. Yin, D. Yang, T. Sun, H. Yu, H.E. Hoster, H.H. Hng, H. Zhang, Q. Yan, Energy Environ. Sci. 6 (2013) 987–993.
[35] D. Rangappa, K.D. Murukanahally, T. Tomai, A. Unemoto, I. Honma, Nano Lett. 12 (2012) 1146–1151.